

Mechanism for Explaining Differences in the Order Parameters of FeAs-Based and FeP-Based Pnictide Superconductors

Ronny Thomale,¹ Christian Platt,² Werner Hanke,² and B. Andrei Bernevig¹

¹*Department of Physics, Princeton University, Princeton, New Jersey 08544, USA*

²*Institute for Theoretical Physics and Astrophysics, University of Würzburg, Am Hubland, D 97074 Würzburg, Germany*

(Received 24 February 2010; revised manuscript received 12 May 2010; published 6 May 2011)

We put forward a scenario that explains the difference between the order-parameter character in arsenide (As) and phosphorous (P) iron-based superconductors. Using functional renormalization group to analyze it in detail, we find that nodal superconductivity on the electron pockets (hole pocket gaps are always nodeless) can naturally appear when the hole pocket at (π, π) in the unfolded Brillouin zone is absent, as is the case in LaOFeP. There, electron-electron interactions render the gap on the electron pockets softly nodal (of s^\pm form). When the pocket of d_{xy} orbital character is present, intraorbital interactions with the d_{xy} part of the electron Fermi surface drives the superconductivity nodeless.

DOI: 10.1103/PhysRevLett.106.187003

PACS numbers: 74.20.Mn, 74.20.Rp, 74.25.Jb

After two years of intense research in the new iron-based superconductors (pnictides) [1], the symmetry of the order parameter is still far from settled. Theoretically, the current opinion converged on an s^\pm order parameter that changes sign between the electron (e) and hole (h) pockets, which comes out of both strong- and weak-coupling pictures of the iron-based superconductors (SC) originating from inter-pocket pair hopping [2–8]. The method of choice in the intermediately correlated pnictides is likely the functional renormalization group (FRG), which systematically takes into account the competing ordering tendencies in the system [8–13]. Previous FRG work gives anisotropic gaps around the e pockets, which, at their smallest value, are close to but do not cross zero [9]. In pnictides such as LaOFeAs, a majority of experiments point to the existence of nodeless isotropic gaps [14,15] on the hole (h) Fermi surface (FS) and also nodeless gaps on the electron (e) FS, albeit with a larger gap anisotropy [16–21]. In contrast, in LaOFeP, a clear majority of experiments support a nodal gap behavior on the e pockets [22,23]. This difference is even more puzzling, since both materials display similar e and h pockets at X and Γ points (see Fig. 1) [24].

In this Letter, we offer an explanation for the difference between the order-parameter character in the As- and P-based compounds. Using FRG on a five-band model of the pnictides with orbital interactions, we find that the gap on the e pockets can undergo a nodal transition if the h pocket at (π, π) (M) is absent. On the basis of RPA calculations, Kuroki *et al.* [25] already argued that the appearance of the FS around (π, π) in the unfolded Brillouin zone is sensitive to the pnictogen height measured from the Fe plane and may drive a nodal or a nodeless pairing. In contrast to the FRG, however, the RPA assumes right from the outset a magnetically driven spin-density wave (SDW) type of pairing interaction. The FRG starts from the “bare” many-body interaction [Eq. (2) below] in the Hamiltonian, and the pairing is dynamically generated by systematically

integrating out the high-energy degrees of freedom including all important fluctuations on equal footing. In the RPA calculation the competition between nodal s^\pm -wave and d -wave pairing is rather subtle and the B_{1g} d -wave solution can win over the nodal s^\pm wave for the LaFePO system [Fig. 16(a) of [25]]. This is neither reflected by experiments nor found in the FRG: here the s^\pm results (even varying them in a rather wide regime) are very robust. Specifically, in the pnictides, the repulsive interaction connects the FS pockets around Γ , X , and, if present, also M points. Though repulsive in the singlet channel, the corresponding contributions yield strong pairing provided the gap function on the two sets of FS have opposite sign. We show in this Letter that the generalization of the original s^\pm -state argument [3,5] acting between Γ and X pockets is also at work for the cases considered here, and explains the propensity to a nodal or nodeless SC gap.

We use a two-dimensional tight-binding model [5] to describe the 1111-type pnictides:

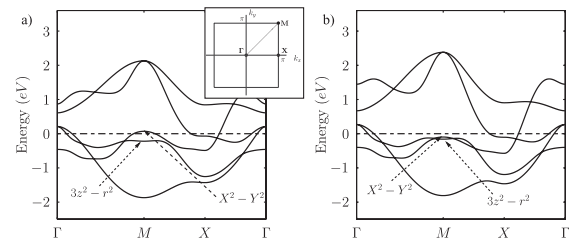


FIG. 1. Band structure for LaOFeAs (a) and LaOFeP (b). (Inset: Brillouin zone.) The tight-binding model for LaOFeAs is given in [5]; the parameters are varied for LaOFeP according to the different pnictogen height parameter [25]. The dashed horizontal lines denote the undoped Fermi level. The major difference between (a) and (b) is the $d_{X^2-Y^2}$ dominated band crossing the Fermi level in (a), but not in (b).

$$H_0 = \sum_{k,s} \sum_{a,b=1}^5 c_{kas}^\dagger K_{ab}(\mathbf{k}) c_{kas}. \quad (1)$$

Here, c denotes electron annihilation operators, a, b the five Fe d orbitals, and s the spin indices. While the main electronic structure of P-based and As-based compounds is very similar, there are certain important differences. Figure 1 shows the band structure of LaOFeAs and LaOFeP, where the latter is obtained by adjusting the parameters in [5] according to the changed pnictogen height from As to P [25]. In the vicinity of the Fermi surface, the most notable difference is the presence or absence of a broad $d_{x^2-y^2}$ (d_{xy})-dominated band at $M = (\pi, \pi)$, in agreement with angle-resolved photoemission spectroscopy data. To account for this difference, we use a five pocket scenario for the As-based and a four pocket scenario for the P-based compounds. We, thus, choose to compare and analyze two generic cases, with or without the h pocket at M , as corresponding to the As-based 1111 (122) and the P-based compounds, respectively.

The interactions in the orbital model are given by

$$H_{\text{int}} = \sum_i \left[U_1 \sum_a n_{i,a\uparrow} n_{i,a\downarrow} + U_2 \sum_{a<b,s,s'} n_{i,as} n_{i,bs'} \right. \\ \left. + \sum_{a<b} \left(J_H \sum_{s,s'} c_{ias}^\dagger c_{ibs'}^\dagger c_{ias} c_{ibs} + J_{\text{pair}} c_{ia\uparrow}^\dagger c_{ia\downarrow}^\dagger c_{ib\downarrow} c_{ib\uparrow} \right) \right], \quad (2)$$

where $n_{i,as}$ denote density operators at site i of spin s in orbital a . We consider intraorbital and interorbital interactions U_1 and U_2 as well as Hund's coupling J_H and pair hopping J_{pair} . In what follows, a physical interaction setting is chosen dominated by intraorbital coupling, $U_1 > U_2 > J_H \sim J_{\text{pair}}$, taking $U_1 = 3.5$ eV, $U_2 = 2.0$ eV, $J_H = J_{\text{pair}} = 0.7$ eV [9]. In terms of interaction scale ratios, this choice roughly corresponds to interaction parameters obtained by constrained RPA *ab initio* calculations [26].

Using FRG [9–11,27,28], we study how the renormalized interaction described by the four-point function (4PF) evolves under integrating high-energy fermionic modes: $V_\Lambda(\mathbf{k}_1, n_1; \mathbf{k}_2, n_2; \mathbf{k}_3, n_3; \mathbf{k}_4, n_4) c_{k_4 n_4 s}^\dagger c_{k_3 n_3 s}^\dagger c_{k_2 n_2 s} c_{k_1 n_1 \bar{s}}$, where the flow parameter is the IR cutoff Λ approaching the Fermi surface, and with \mathbf{k}_1 to \mathbf{k}_4 the incoming and outgoing momenta, and n_1 to n_4 the band index. Because of the spin rotational invariance of interactions, we constrain ourselves to the $S^z = 0$ subspace of incoming momenta $\mathbf{k}_1, \mathbf{k}_2$ (and outgoing $\mathbf{k}_3, \mathbf{k}_4$) and generate the singlet and triplet channel by symmetrization and antisymmetrization of the 4PF V_Λ [27]. The starting conditions are given by the bandwidth serving as an UV cutoff, with the bare initial interactions for the 4PF. The diverging channels of the 4PF under the flow to the Fermi surface signal the nature of the instability, and the corresponding Λ_c serves as an upper bound for the transition temperature T_c . For a

given instability characterized by some order parameter $\hat{O}_\mathbf{k}$ (the most important example of which is the SC instability $\hat{O}_\mathbf{k}^{\text{SC}} = c_\mathbf{k} c_{-\mathbf{k}}$ in our case), the 4PF in the particular ordering channel can be written as $\sum_{\mathbf{k}, \mathbf{p}} V_\Lambda(\mathbf{k}, \mathbf{p}) [\hat{O}_\mathbf{k}^\dagger \hat{O}_\mathbf{p}]$ [12]. Accordingly, the 4PF in the Cooper channel can be decomposed into different eigenmode contributions $V_\Lambda^{\text{SC}}(\mathbf{k}, -\mathbf{k}, \mathbf{p}) = \sum_i c_i^{\text{SC}}(\Lambda) f^{\text{SC},i}(\mathbf{k}) f^{\text{SC},i}(\mathbf{p})$, where i is a symmetry decomposition index ordered such that $i = 1$ labels the leading order; i.e., the leading instability of the SC channel corresponds to the eigenvalue $c_1^{\text{SC}}(\Lambda)$ first diverging under the flow of Λ . $f^{\text{SC},i}(\mathbf{k})$ is the SC form factor of pairing mode i revealing the SC pairing symmetry and is computed along the discretized Fermi surfaces [leading instability form factors are plotted in Figs. 2(a) and 3(a)].

As-based compounds.—For the As-based setting (Fig. 2), we find that the s^\pm instability, giving rise to different gap signs on h versus e pockets, is the leading instability of the model at moderate doping. The setup resembles the situation studied in [9], which we also studied with a more detailed tight-binding structure beyond 5th next-nearest neighbors [5]. We also find a nodeless s^\pm SC leading instability. In addition, we can identify the h pocket at M to play a major role in contributing to the fully gapped s wave and to a sign change from h to e pockets (Fig. 2). In particular, we study the orbital content in detail and analyze how the pairing instability distributes over the different orbitals [Fig. 2(d)]. For this, we consider the 4PF in orbital space,

$$V_{c,d \rightarrow a,b}^{\text{orb}} = \sum_{n_1, \dots, n_4=1}^5 \{ V_\Lambda(\mathbf{k}_1, n_1; \mathbf{k}_2, n_2; \mathbf{k}_3, n_3; \mathbf{k}_4, n_4) \\ \times u_{an_1}^*(\mathbf{k}_1) u_{bn_2}^*(\mathbf{k}_2) u_{cn_3}(\mathbf{k}_3) u_{dn_4}(\mathbf{k}_4) \}, \quad (3)$$

where the u 's denote the different orbital components of the band vectors [29]. The matrix shown in Fig. 2(d) gives the leading eigenvalue contributions of $V_{\Lambda,(a,b)}^{\text{SC}}(\mathbf{k}, \mathbf{p}) c_{k,a}^\dagger c_{-k,a}^\dagger c_{p,b} c_{-p,b}$, i.e., in the Cooper channel of (3) where we constrain ourselves to the dominant processes of intra-orbital pairing $(a, a) \rightarrow (b, b)$. As above, we decompose it into different form factor contributions $\sum_i c_i^{\text{SC}}(\Lambda) f_{(a,b)}^{i,\text{SC}}(\mathbf{k}) f_{(a,b)}^{i,\text{SC}}(\mathbf{p})$, where the leading eigenvalues at Λ_c for the different (a, b) are given in Figs. 2(d) and 3(d). Intraorbital scatterings between the d_{xz} (or d_{yz}) orbital-dominated parts of the e and Γ h pockets are most important (Fig. 2). They favor an s^\pm SC instability, as was also found in [9]. However, the leading eigenvalue in the As scenario comes from the diagonal part of the $d_{x^2-y^2}$ orbital. Pointing in the direction of the $\Gamma \leftrightarrow X$ path, the e pocket has a high concentration of the $d_{x^2-y^2}$ orbital. This part of the e pocket then scatters strongly with the h pocket at the M point, which is dominated by the $d_{x^2-y^2}$ orbital band. The intraorbital repulsion related to the latter scattering prefers again an s^\pm -type pairing between the h pocket at M and the e pockets, which

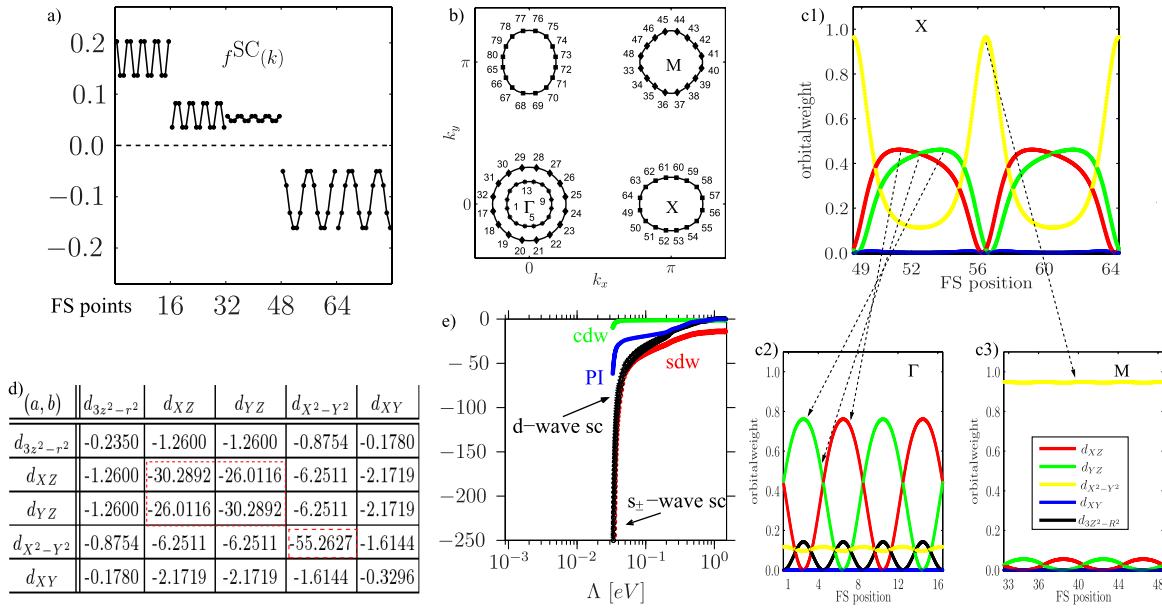


FIG. 2 (color online). Five pocket scenario for LaOFeAs. (a) Plot of the SC form factor gap $f^{\text{SC}}(k)$ versus the patching indices (momenta) shown in (b). The gap on the outer h pocket at Γ is smaller than that of the inner h pocket and of the same order as the M -pocket gap. The gap on the e pockets is very anisotropic but nodeless and of opposite sign. (c1)–(c3) Orbital weight distribution on the different pockets [inner h pocket at Γ is similar to (c2) shifted by 90°]. Dashed arrows indicate relevant intraorbital scatterings. (d) Leading orbital SC instability eigenvalues $c_{i,(a,b)}^{\text{SC}}(\Lambda_c)$ from (3). $d_{XZ,YZ}$ and $d_{X^2-Y^2}$ scattering dominates. (e) Flow of leading instability eigenvalues [charge density wave (CDW), Pomeranchuk instability (PI), SDW, and SC]. The leading instability is s^\pm SC at $\Lambda_c \approx 0.03$ eV, B_{1g} d -wave SC and SDW diverge closely (hardly distinguishable on the log scale).

reinforces the already present s^\pm between the Γ h pockets and the X (X') e pockets. Assuming that U_1 is the dominant interaction, the three h pockets display a gap of identical sign: the two Γ pockets which are not nested with each other have the same gap sign, and are of different orbital content than the h pocket at M . However, the e pockets contain contributions from all three relevant d orbitals. Therefore, the e pockets scatter strongly through U_1 with all three h pockets, which enhances the s^\pm character of the gap. So, in summary of the As scenario, having the SC pair state orthogonal to the repulsive interaction [30] induced by the presence of the additional M pocket further increases the s^\pm gap between e and h pockets. The h pocket at M is also responsible for the strong SDW signal [Fig. 2(e)], as the nesting wave vector $M \leftrightarrow X$ is the same as $\Gamma \leftrightarrow X$.

P-based compounds.—Here, the physical picture changes even qualitatively. As shown in Fig. 3, we find a nodal s^\pm scenario for the P-based compounds, with lower critical divergence scale $\Lambda_c \sim T_c$ and less SDW-type fluctuations. The absence of the M h pocket removes the intraorbital scattering to the e pockets. This gives way to previously subleading scattering channels such as, in particular, e - e scattering between the $d_{X^2-Y^2}$ -dominated parts of the e pockets, but also pair hopping from the h pockets at Γ to the e pockets. The former acts between the k points of the gap function on the e pockets given by the peaks and the valleys [Fig. 3(a)] increasing the anisotropy and

eventually giving them different signs, thus creating a nodal state. Even if the $d_{3z^2-r^2}$ -dominated band at M [Fig. 1(b)] were shifted to the Fermi level, the situation remains nearly unchanged as this pocket does not share its orbital content with any other pocket, and hence interactions driven by U_1 are suppressed.

To further substantiate our conclusions, we perform a large sweep in parameter space to resolve the evolution of the SC form factor upon varying the interaction parameters [29]. For the validity of the scenarios above, it is essential that U_1 be the leading energy scale $U_1/U_2 > 1.3$. For physically relevant parameters, $U_1/J_H > 4$, Hund's coupling does not change the essential structure of the SC form factor. J_{pair} is a sensitive interaction parameter for the P-based compounds. We find that the nodal SC form factor is valid for the parameter regime $U_1/J_{\text{pair}} > 4$. Below, the interplay with the e - e scattering, driven by U_1 , yields a SC form factor with reduced nodal propensity.

From the *ab initio* data stated before, we get $U_1/U_2 \approx 1.5$, $U_1/J_H = U_1/J_{\text{pair}} \approx 6.5$. As such, the parameter regime of the As-based and P-based compounds lies in the regime of applicability of our theory, which is consistent with experiment: in the P-based compounds, we find (i) a lower divergence scale and hence lower T_c compared to As-based compounds, (ii) significantly enhanced low energy density of states in the (hence nodal) superconducting phase, and (iii) reduced SDW-type fluctuations, which, even at pronounced nesting, are insufficient to drive the

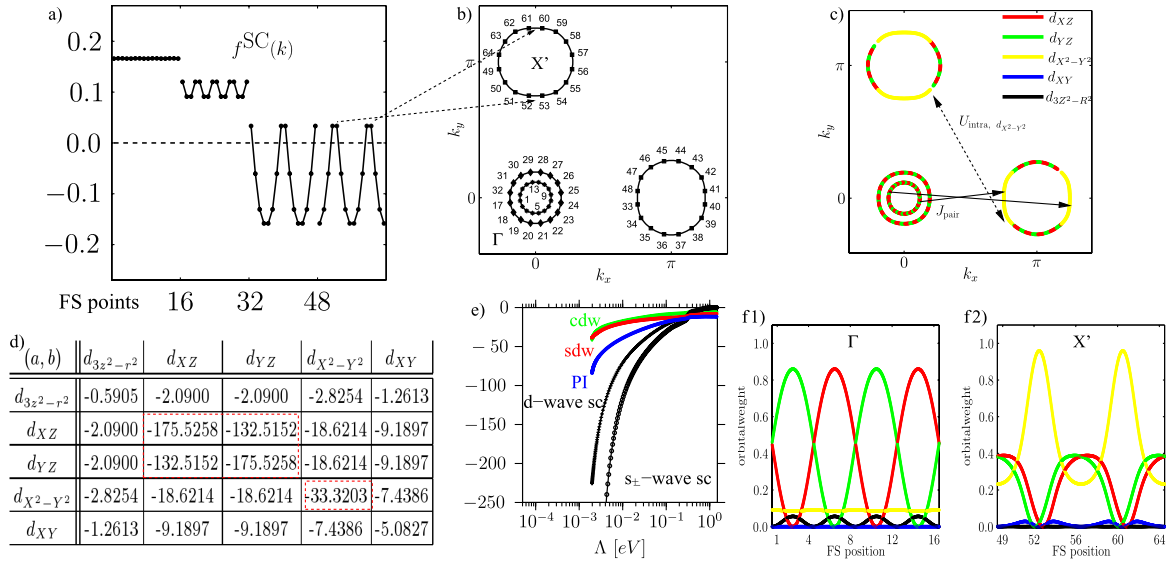


FIG. 3 (color online). Four pocket scenario for LaOFeP. (a) s^\pm SC form factor, with FS patches given in (b); the $d_{X^2-Y^2}$ -dominated h pocket at M is absent. The h pockets at Γ are gapped and isotropic. The e pockets show strong anisotropy, being nodal on the pocket tips indicated in Fig. 2(b) by dashed arrows. (c) Relevant pair scattering and intraorbital processes between different e pockets [orbital weights of the pockets are shown in (f1) and (f2)]. (d) Orbital decomposition of the SC instability: large $d_{XZ,YZ}$ and less relevant $d_{X^2-Y^2}$ contribution. (e) Flow of leading instability eigenvalues [notation as in Fig. 2(e)]; $\Lambda_c \approx 0.002$ eV is smaller than in Fig. 2.

system to a leading magnetic SDW instability [22–24]. The absence of the hole pocket at M also manifests itself in the orbital decomposition of the pairing instability [Fig. 3(d)]; the diagonal contribution of $d_{X^2-Y^2}$, in comparison to $d_{XZ,YZ}$, is reduced.

In summary, we find that the broad band at the unfolded M point plays the major role in explaining the drastic change of SC properties from the As-based to the P-based 1111 compounds, rendering the former nodeless and the latter nodal. The nodes that appear in the P-based compounds are driven by anisotropy of the electron pockets.

We thank C. Honerkamp, J. Hu, K. Kuroki, D.-H. Lee, D. Scalapino, Z. Tesanovic, A. Vishwanath, and F. Wang for discussions. R.T. is supported by the Humboldt Foundation. R.T., C.P., and W.H. are supported by DFG-SPP 1458/1, C.P. and W.H. by DFG-FOR 538. B. A. B. is supported by Princeton Startup Funds, Sloan Foundation, NSF DMR-095242, and NSF DMR-0819860.

Note added.—Recently, we became aware of a related independent work studying LaOFeP through FRG [13]. Our data range and interpretation of the numerical results contains and exceeds the case studied there.

- [1] Y. Kamihara *et al.*, *J. Am. Chem. Soc.* **130**, 3296 (2008).
- [2] K. Seo, B. A. Bernevig, and J. Hu, *Phys. Rev. Lett.* **101**, 206404 (2008).
- [3] I. I. Mazin *et al.*, *Phys. Rev. Lett.* **101**, 057003 (2008).
- [4] S. Graser *et al.*, *New J. Phys.* **11**, 025016 (2009).
- [5] K. Kuroki *et al.*, *Phys. Rev. Lett.* **101**, 087004 (2008).
- [6] V. Stanev, J. Kang, and Z. Tesanovic, *Phys. Rev. B* **78**, 184509 (2008).

- [7] M. M. Korshunov and I. Eremin, *Phys. Rev. B* **78**, 140509 (2008).
- [8] A. V. Chubukov, D. V. Efremov, and I. Eremin, *Phys. Rev. B* **78**, 134512 (2008).
- [9] F. Wang *et al.*, *Phys. Rev. Lett.* **102**, 047005 (2009).
- [10] C. Platt, C. Honerkamp, and W. Hanke, *New J. Phys.* **11**, 055058 (2009).
- [11] R. Thomale *et al.*, *Phys. Rev. B* **80**, 180505 (2009).
- [12] H. Zhai, F. Wang, and D.-H. Lee, *Phys. Rev. B* **80**, 064517 (2009).
- [13] F. Wang, H. Zhai, and D.-H. Lee, *Phys. Rev. B* **81**, 184512 (2010).
- [14] L. Wray *et al.*, *Phys. Rev. B* **78**, 184508 (2008).
- [15] H. Ding *et al.*, *Europhys. Lett.* **83**, 47001 (2008).
- [16] K. Matano *et al.*, *Europhys. Lett.* **83**, 57001 (2008).
- [17] M. M. Parish, J. Hu, and B. A. Bernevig, *Phys. Rev. B* **78**, 144514 (2008).
- [18] K. Hashimoto *et al.*, *Phys. Rev. Lett.* **102**, 207001 (2009).
- [19] L. Malone *et al.*, *Phys. Rev. B* **79**, 140501 (2009).
- [20] M. A. Tanatar *et al.*, *Phys. Rev. Lett.* **104**, 067002 (2010).
- [21] J. G. Checkelsky *et al.*, arXiv:0811.4668.
- [22] M. Yamashita *et al.*, *Phys. Rev. B* **80**, 220509 (2009).
- [23] C. W. Hicks *et al.*, *Phys. Rev. Lett.* **103**, 127003 (2009).
- [24] D. H. Lu *et al.*, *Physica (Amsterdam)* **469C**, 452 (2009).
- [25] K. Kuroki *et al.*, *Phys. Rev. B* **79**, 224511 (2009).
- [26] T. Miyake *et al.*, *J. Phys. Soc. Jpn.* **79**, 044705 (2010).
- [27] C. Honerkamp *et al.*, *Phys. Rev. B* **63**, 035109 (2001).
- [28] R. Shankar, *Rev. Mod. Phys.* **66**, 129 (1994).
- [29] See supplemental material at <http://link.aps.org/supplemental/10.1103/PhysRevLett.106.187003> for detailed parameter studies complementary to the results shown and a short derivation of Eq. (3).
- [30] P. W. Anderson, *Science* **316**, 1705 (2007).